Performance prediction of the combined cycle power plant with inlet air heating under part load conditions

Shucheng Wang[a,c,*], Zhitan Liu[b], Rasmus Cordtz[c], Muhammad Imran[d] ,Zhongguang Fu[a]

[a] *Key Laboratory of Condition Monitoring and Control for Power Plant Equipment, Ministry of Education, North China Electric Power University, Beijing 102206, China*

[b] *Guodian Science and Technology Research Institute, China Energy Investment Corporation, Nanjing 210031,China*

[c] *Section of Thermal Energy, Department of Mechanical Engineering, Technical University of Denmark, Building 403, Nils Koppels Allé, 2800 Kgs. Lyngby, Denmark*

[d] *Mechanical Engineering & Design Group, School of Engineering and Applied Science, Aston University, Aston Triangle, Birmingham B4 7ET, UK*

Abstract

A combined cycle power plant with inlet air heating (CCPP-IAH) system is proposed to solve the problems of ice and humidity blockages in winter climate. The performance of the CCPP-IAH system under part load conditions is analyzed via both experimental and simulation methods. The application of the inlet air heating technology significantly improves the part load efficiency and enhances the operational safety of the combined cycle power plant under complex meteorological conditions. Results show that a higher inlet air temperature will contribute a lower gas turbine thermal efficiency for proposed system. However, the heated inlet air by the recovered energy in heat recovery steam generator raises efficiencies for both the heat recovery steam generator and the overall system. The fuel consumption drops by 0.02 kg/s and 0.03 kg/s under the power load of 65 % and 80 %, respectively. The inlet air humidity decrease to 30 % under the heated inlet air temperature of 303 K. Moreover, the exergy destruction for both Brayton cycle part and Rankine cycle part decrease with the inlet air temperature increasing. The daily fossil fuel will raise up to 2.9 ton/day and to 5.1 ton/day under the power load of 65 % and 80 %, respectively. The annual economic benefit from energy saving is more than \$ 5.88×10^5 and the payback period is less than 3 years.

Keywords: CCPP; Combined cycle power plant; Inlet air heating; Optimization; Part load; Experimental test;

1. Introduction

With the world's population growth and substantial economic development the energy demand and associated air pollution is increasing rapidly. Based on a survey of the International Energy Agency in 2017, the global energy demand will rise by 30 % in 2040 [1]. Hence, it is of particular importance to adopt efficient and cleaner energy supply strategies to cover the energy demand [2, 3]. In recent years, gas-fired power plants involving a single gas turbine and combined cycle power plant (CCPP) have developed rapidly due to its high thermal efficiency, lower emissions and strong peak load shaving ability [4]. Therefore, gas-fired power systems are globally recognized as the most efficient converters from fossil fuel to electricity [5].

1.1 Literature review

Since most gas-fired power plants are highly powerful, even a small improvement yields a power gain in the MW range [6]. In order to improve the efficiency of such systems numerous concepts have been introduced. Ibrahim et al.[7] analyzed the performance of a gas turbine (GT) based power plant under different ambient temperatures using the first and second law of thermodynamics. The main components of the power system were modeled and the results showed that the combustion chamber had the largest irreversible energy loss. They also revealed that a reduction of the inlet air temperature (*IAT*) can improve the overall system efficiency significantly. Maheshwari and Singh [8] focused on thermodynamic analysis of CCPP under eight different configurations. They resulted that the maximum energy efficiency of 54.9 % was achieved by utilizing a reheater in the CCPP system. Sanaye et al. [9] investigated and optimized a GT-based combined cooling heating and power (CCHP) system using 4E (Energy, Exergy, Environmental and Economic) methods. Optimization results revealed that the *IAT* of 291.5 K and steam injection of 1.8 % into the combustion chamber were selected as the optimum points. Mohapatra and Sanjay [10]performed an exergy evaluation on a CCPP with an inlet air cooling system to increase the exergy efficiency of overall plant. Results showed that the combustion chamber had the highest exergy improvement potential. Moreover, the total exergy destruction was reduced by increasing the turbine inlet temperature and decreasing the compressor inlet temperature.

Additionally, several technological means are proposed to enhance the part load performance of GT-based power plants. Haglind [11] presented and compared the properties of variable geometry on the part load performance of two selected gas turbines. Results indicated the GT with two-shaft had better part load performance than the single-shaft one. Li et al.[12] proposed a backpressure adjustable method for a CCPP system to improve the off-design performance of the overall system. The simulation results revealed that the proposed method can significantly broaden the load range and increase the overall system efficiency by 1.76 %. EI-Shazly et al. [13] proposed an evaporative cooler system for a GT and compared it with a conventional absorption chiller under a wide temperature range. An increment of 2.03 MW is gained with the evaporative cooler system. Huang et al. [14] proposed a steam injection method for a GT-based CCHP system at an off-design condition. The injection of steam can significantly improve the GT efficiency and the overall system had the best performance among other approaches.

A critical issue concerning GT-based power plants is that the power output decreases considerably when the ambient temperature increases [2, 15, 16]. Especially in the summer, the ambient temperature can be far from the design temperature. As a result, the thermal efficiency as well as the power output of the GT reduces. It has been reported that a power plant in Iran generates only 80 % of the rated capacity during summer season [17]. Therefore, to enhance the performance and produce additional power during hot seasons, inlet air cooling is a widely used technology in CCPP systems.

Baakeem et al. [18] analyzed several inlet air cooling technologies regarding fuel consumption rate, thermal efficiency and gas turbine power output. They found that a hybrid sub-cooling system showed the best performance. Brzeczek and Job [19] presented the impact of steam cooling in both gas turbine and overall power plant. The recovered energy from the intercooler was further utilized by an additional Rankine cycle. Results showed that the proposed system improved electrical efficiency by 7 %, which was higher than the classical open-air cooling system. Kwon et al. [20] selected dual cooling for a CCPP system and concluded that the proposed method produces a higher power output of 8.2 % compared to other inlet air cooling systems. Li et al. [21] proposed an inlet air cooling system using the evaporative cooling energy from liquefied natural gas for a CCPP system. The off-design performance was evaluated under different ambient conditions and the modified CCHP system produced a higher output in the range of 1.83 %-14.4 %.

The above research shows that it is overwhelmingly beneficial to reduce the *IAT* of the GT system compressor in order to improve part load performances. However, it seems that little research has concerned the utilization of inlet air heating (using recovered energy from HRSG) for CCPP under part load conditions.

1.2 Motivation

The CCPPs are considered viable technology for peak shaving. This means that the systems will run at part load conditions for most of the time. Therefore, improving the part load performance and meet the anti-freezing requirement (in winter) are particularly important. Nevertheless, it seems that no publications have investigated this significant issue. In this paper, a novel CCPP system with inlet air heating (CCPP-IAH) is proposed and is considered as an effective way to improve the part load performance of GT-based power systems.

The main contributions of the present work are:

- The proposed mode of the CCPP-IAH is established and based on a real system in Tianjin city to solve the issuers of ice and humidity blockages in the inlet air system.
- The part-load performance of the proposed system was investigated experimentally and by simulation methods, the performance is compared with a conventional CCPP system.
- The exergy destruction of main components of the proposed CCPP-IAH system was analyzed. Furthermore, the components were divided into a Brayton cycle part and a Rankine cycle part to better understand the potential improvements.
- The experimental data combined with simulated results provided a valuable method to avoid the issues of ice and humidity blockages in the inlet air system of the CCPPs. The application of the IAH technology significantly enhances the operation of the CCPPs under complex meteorological conditions.

2. System description

2.1 CCPP system

Tianjin is a coastal city and it is located in the north part of China (117 °E, 39 °N). The average and the minimum temperature in the winter is 277.8 K and 259.6 K respectively. The average relative humidity is 56.4%. As a result, freezing in the inlet air system of CCPPs will occur in wintertime, which increases the pressure drop and lowers the power output. The CCPP under investigation consists of an E-class gas turbine, a steam turbine and a HRSG. The gas turbine is produced by General Electricand typed with the number PG9171E [23]. Design data of the PG9171E are listed in Table 1. The steam turbine was produced by Nanjing Turbine & Electric Machinery Group and has the type number LCZ65-5.8/0.45/0.4 [24]. The HRSG is a double pressure combustion boiler produced by AE&E Nanjing boiler Co.,Ltd [25].

The gas-fired power plant was constructed to provide electricity, hot water and space heating in winter for nearby consumers. Since Tianjin is a coastal city and the relative humidity in winter is high, there will be freezing phenomenon in the inlet air system of CCPP, which increases the pressure loss and drops the power output. On the other hand, the gas-fired power plant is used for peak shaving and it is operated under part load conditions most of the time. Hence, the CCPP was modified for anti-freezing and improving its part load performance. The schematic diagram of the CCPP with inlet air heating system is shown in Figure 1.

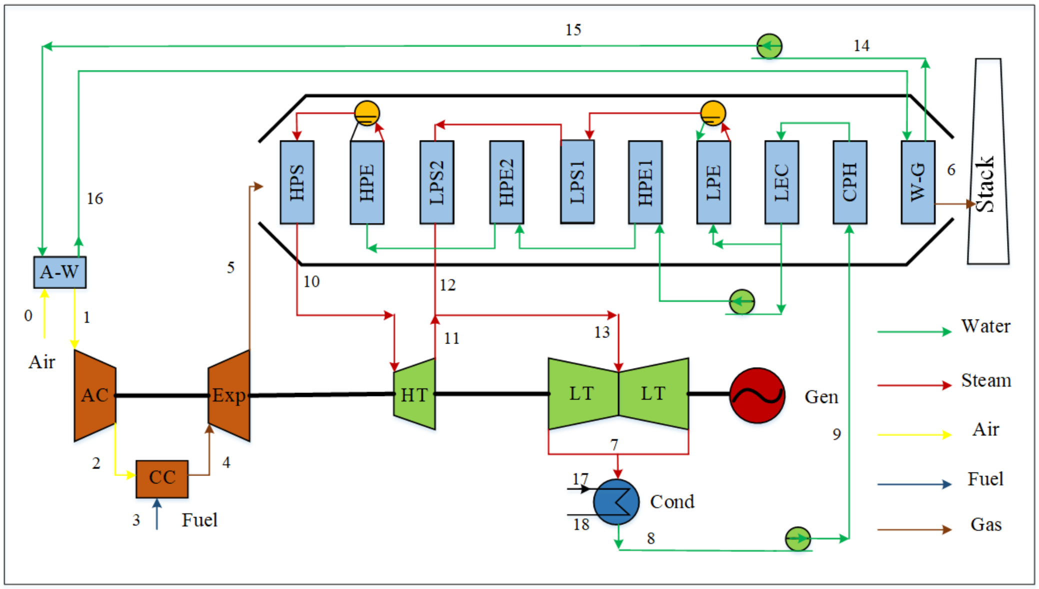

Figure 1. Schematic diagram of the CCPP with inlet air heating system.

Table 1.

Design data of GT under ISO conditions.

Descriptions	Unit	Power loads		
		100 %	75 %	50 %
Ambient temperature	K	288	288	288
Ambient pressure	MPa	0.1	0.1	0.1
Relative humidity	%	60	60	60
Power factor		0.85	0.85	0.85
GT power output	MW	126.8	95.1	63.4
GT heat rate	kJ/kWh	10630	11610	13980
GT efficiency	%	33.87	31.01	25.75
GT exhaust gas temperature	K	819.7	851.2	866.3
GT exhaust gas mass flow rate	kg/s	416	329.7	274.3
HRSG high-pressure steam pressure	MPa	6.1	6.1	6.1
HRSG high-pressure steam temperature	K	797	812	812
HRSG low-pressure steam pressure	MPa	0.53	0.53	0.53
HRSG low-pressure steam temperature	K	488	483	480
ST power output	MW	64.66	57.06	49.5
ST heat rate	kJ/kWh	3706	3692	3677
CCPP power output	MW	191.46	152.16	112.95
CCPP heat rate	kJ/kWh	7040	7256	7847.4
CCPP efficiency	%	51.14	49.61	45.87

2.2 IAH system description

As shown in Figure 2, a 2.5 meter-wide anti-freezing unit was mounted in the front of the inlet air system. The existing rainproof cover was placed in the front of the anti-freezing unit. A group of heat exchangers (A-W) were added inside the anti-freezing unit to supply the inlet air heating. In addition, a set of hot water pipelines were used to connect the heat exchangers of the anti-freezing warehouse and the HRSG. A water-gas exchanger (W-G) with a 7 MW capacity already existed in the HRSG before the modification. The water-gas exchanger was initially used to produce hot water and provide space heating. The heating water from the HRSG enters from the top of the A-W heat exchangers and flows out though the bottom pipelines. Furthermore, thermocouples were placed to measure the temperature of the inlet air. The full structure of the IAH system is shown in Figure 3.

The air is heated by the air-water exchanger (A-W) and compressed by the air compressor (AC). The compressed air is used to burn the fuel in the combustion chamber (CC). The generated high-pressure gas drives the gas turbine and the electric generator. The high temperature exhaust form the GT (~833 K) enters the HRSG and heats feed water in two different pressure quality/level steam flows; the high-pressure steam (6.1 MPa) and the low-pressure steam (0.53 MPa). Thereafter the steams enters the steam turbines to produce additional work/electricity.

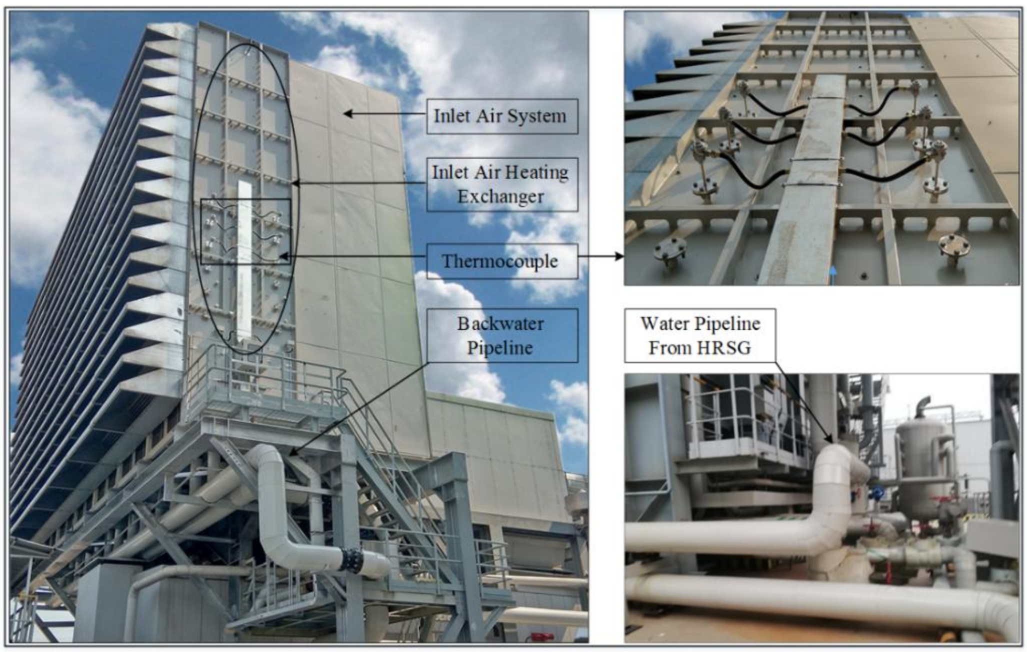

Figure 2. The inlet air heating system for CCPP.

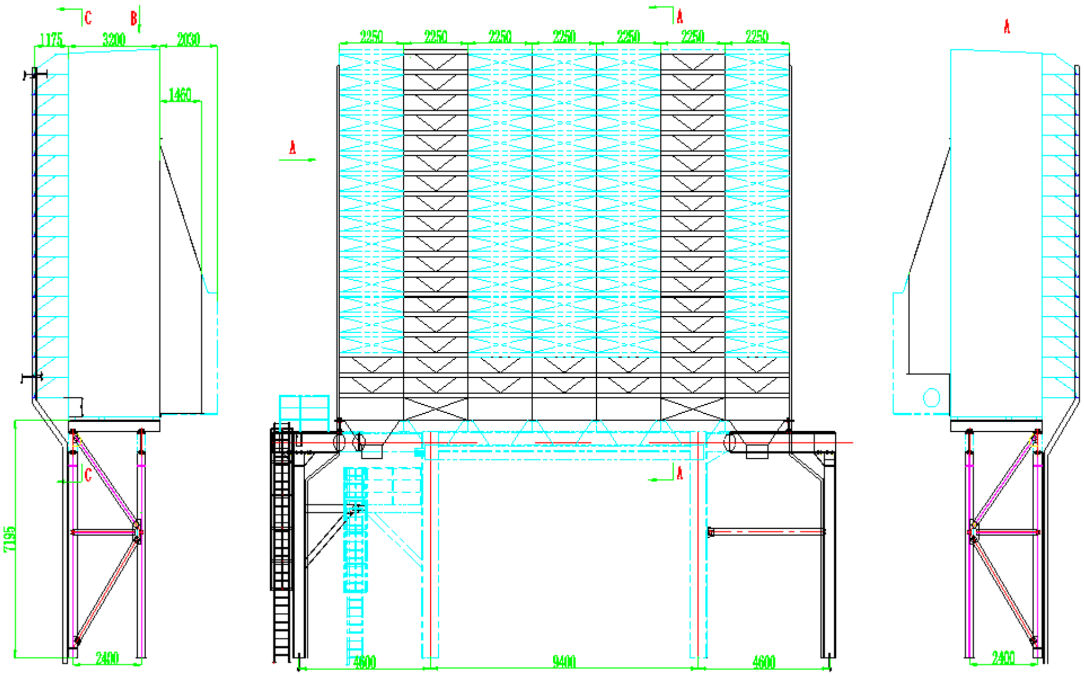

Figure 3. The structure of the inlet air heating system.

3. Energy and exergy analysis of CCPP-IAH system

In this study, a simulated model is constructed and validated with the practical model. Then, the energy analysis (fuel consumption, heat rate, energy efficiency, air humidity), exergy analysis (exergy destruction of components and the overall system), economic analysis (fossil fuel saving and dynamic payback period) are considered to better understand the system performance potential improvement under both different power load and the *IAT*. The methodology process of proposed CCPP-IAH system is shown in Figure 4.

3.1 Energy analysis

The model of the CCPP-IAH system was developed with the software Ebsilon Professional [22] and the state of the working media (temperature, pressure, mass flow rate, enthalpy and exergy) were determined prior to the energy and exergy analysis.

3.1.1 Compressor

The overall CCPP consists of the GT, steam turbine (ST) and the HRSG. The GT alone consists of a gas turbine, compressor, combustion chamber (CC) and an expander. The performance of the compressor is highly affected by the inlet air temperature (T_1). The outlet temperature (T_2), outlet pressure (P_2) and the power consumption ($\dot{W}_{\mathrm{AC}}$) of the compressor is calculated by [23-25]:

$$T_2 = T_1 \times \left[1 + \frac{1}{\eta_{\mathrm{AC}}} \left(r_{\mathrm{AC}}^{\frac{k-1}{k}-1} - 1 \right) \right] \tag{1}$$

$$P_2 = P_1 \times \left[\frac{\eta_{\mathrm{AC}}(T_2 - 1) + 1}{T_1} \right]^{\frac{k}{k-1}} \quad (2)$$

$$\dot{W}_{\mathrm{AC}} = \dot{m}_{\mathrm{a}} \times c_{\mathrm{pa}} \times (T_2 - T_1) \quad (3)$$

η_{AC} is the efficiency of the compressor, k is the specific heat ratio, r_{AC} is the pressure ratio, $\dot{m}_{\mathrm{a}}$ is the mass flow rate of the inlet air and c_{pa} is the specific heat of air, which can be further calculated by:

$$c_{\mathrm{pa}}(T) = 1.048 - (\frac{1.83T}{10^4}) + (\frac{9.45T^2}{10^7}) - (\frac{5.49T^3}{10^{10}}) + (\frac{7.92T^4}{10^{14}}) \quad (4)$$

3.1.2 Combustion chamber

The compressed air and natural gas are burned in the compressor chamber, the energy equation can be written:

$$\dot{m}_{\mathrm{a}} \times h_2 + \eta_{\mathrm{CC}} \times \dot{m}_{\mathrm{f}} \times LHV_{\mathrm{f}} = \dot{m}_g \times h_4 \quad (5)$$

$$\dot{m}_{\mathrm{a}} + \dot{m}_{\mathrm{f}} = \dot{m}_g \quad (6)$$

where h_2 and h_4 are the enthalpy of the inlet air and outlet gas of the CC, the η_{CC} is the efficiency of the CC, $\dot{m}_g$ is the mass flow rate of flue gas. Moreover, the LHV_{f} is the lower heating value of the fuel that can be calculated by the fuel composition shown in Table 2.

3.1.3 Expander

The pressurized hot exhaust gas from the CC with temperature (T_4) is expanded to produce useful power. The outlet temperature of the expander (T_5) and the produced power ($\dot{W}_{\mathrm{GT}}$) is calculated by:

$$T_5 = T_4 \times \left[1 - \eta_{\mathrm{Exp}} + \eta_{\mathrm{Exp}} \left(\frac{P_4}{P_5} \right)^{\frac{k-1}{k}} \right] \quad (7)$$

$$\dot{W}_{\mathrm{GT}} = \dot{m}_{\mathrm{g}} \times c_{\mathrm{pg}} \times (T_4 - T_5) \quad (8)$$

where the c_{pg} is the specific heat of the turbine exhaust gas:

$$c_{\mathrm{pg}} = 0.991615 + \left(\frac{6.99703T}{10^5} \right) + \left(\frac{2.7129T^2}{10^7} \right) - \left(\frac{1.22442T^3}{10^{10}} \right) \quad (9)$$

3.1.4 HRSG

The HRSG is used to recover heat from the GT exhaust gas (~833 K). In the HRSG the exhaust gas is used to heat feed water into the high-pressure steam (6.1 MPa) and the low pressure steam (0.53 MPa). The energy balance can be expressed as [26]:

$$\dot{m}_5 \times h_5 - \dot{m}_6 \times h_6 = \dot{m}_{10} \times h_{10} + \dot{m}_{13} \times h_{13} \tag{10}$$

where, the $\dot{m}_5$, $\dot{m}_6$, $\dot{m}_{10}$ $\dot{m}_{13}$ are the exhaust mass flow rate from the GT; mass flow rate of exhaust gas to the stack; mass flow rate of the high pressure steam of HRSG; mass flow rate of low-pressure steam of HRSG respectively.

3.1.5 Steam turbine

The power output of the ST can be calculated by the energy balance equation:

$$\dot{W}_{\mathrm{ST}} = \eta_{\mathrm{ST}} \times (\dot{m}_{10} \times h_{10} - \dot{m}_{11} \times h_{11} + \dot{m}_{13} \times h_{13} - \dot{m}_7 \times h_7) \tag{11}$$

3.1.6 Condenser

The condenser is basically a heat exchanger which condenses the exhaust steam of ST into liquid water. The energy balance equation of the condenser is [27, 28]:

$$\dot{m}_7 \times h_7 - \dot{m}_{17} \times h_{17} = \dot{m}_8 \times h_8 + \dot{m}_{18} \times h_{18} \tag{12}$$

3.1.7 A-W heat exchanger

The air-water (A-W) heat exchanger is designed to heat the inlet air in winter, the outlet temperature (T_1) of the A-W can calculate from:

$$\dot{m}_{\mathrm{a}} \times c_{\mathrm{pa}} (T_1 - T_0) = \dot{m}_{15} \times h_{15} - \dot{m}_{16} \times h_{16} \tag{13}$$

where $\dot{m}_{15}, \dot{m}_{16}$ are the mass flow rate of the inlet and outlet water of the A-W heat exchanger.

3.1.10 Thermal efficiency and heat rate

The GT efficiency (η_{GT}), HRSG efficiency (η_{HRSG}) and the overall proposed CCPP efficiency (η_{CCPP}) is calculated by the following equations [29, 30]:

$$\eta_{\mathrm{GT}} = \frac{\dot{W}_{\mathrm{GT}}}{\dot{m}_{\mathrm{f}} \times LHV_{\mathrm{f}}} \times 100\% \tag{14}$$

$$\eta_{\mathrm{HRSG}} = \frac{T_5 - T_6}{T_5 - T_0} \times 100\% \tag{15}$$

$$\eta_{\mathrm{CCPP}} = \frac{\dot{W}_{\mathrm{GT}} + \dot{W}_{\mathrm{ST}}}{\dot{m}_{\mathrm{f}} \times LHV_{\mathrm{f}}} \times 100\% \tag{16}$$

Similarly, the GT heat rate ($\dot{H}_{\mathrm{GT}}$) and the overall proposed CCPP heat rate ($\dot{H}_{\mathrm{CCPP}}$) can be calculated by the following equations:

$$\dot{H}_{\mathrm{GT}} = \frac{3600 \times \dot{m}_{\mathrm{f}} \times LHV_{\mathrm{f}}}{\dot{W}_{\mathrm{GT}}} \times 100\% \tag{17}$$

$$\dot{H}_{\mathrm{CCPP}} = \frac{3600 \times \dot{m}_{\mathrm{f}} \times LHV_{\mathrm{f}}}{\dot{W}_{\mathrm{GT}} + \dot{W}_{\mathrm{ST}}} \times 100\% \tag{18}$$

3.2 Exergy analysis

The exergy destruction ($\dot{E}_{\mathrm{D},k}$) of any component (*k)* in the system can be calculated as the difference between “input exergy” ($\dot{E}_{\mathrm{F},k}$) and the “Output/product exergy” ($\dot{E}_{\mathrm{P},k}$) as shown in Eq. (19). Moreover, the exergy destruction ratio ($y_{\mathrm{D},k}$) can be defined as the ratio of $\dot{E}_{\mathrm{D},k}$ and $\dot{E}_{\mathrm{F},k}$ Eq. (20) [6, 7, 31].

$$\dot{E}_{\mathrm{D},k} = \dot{E}_{\mathrm{F},k} - \dot{E}_{\mathrm{P},k} \tag{19}$$

$$y_{\mathrm{D},k} = \frac{\dot{E}_{\mathrm{D},k}}{\dot{E}_{\mathrm{F},k}} \times 100\% \tag{20}$$

More specifically, the exergy destruction of main components in the proposed CCPP-IAH system are calculated using the following equations [16, 32].

3.2.1 Compressor

$$\dot{E}_{\mathrm{D,AC}} = \dot{E}_1 + \dot{W}_{\mathrm{AC}} - \dot{E}_2 \tag{21}$$

3.2.2 Combustion chamber [33]

$$\dot{E}_{\mathrm{D,CC}} = \dot{E}_2 + \dot{E}_{\mathrm{fuel}} - \dot{E}_4 \tag{22}$$

where $\dot{E}_{\mathrm{fuel}}$ is the chemical exergy of the fossil fuel (natural gas), which can be calculated by the following equation:

$$\dot{E}_{\mathrm{fuel}} = \xi \times \dot{m}_{\mathrm{f}} \times LHV_{\mathrm{f}} \tag{23}$$

where LHV_{f} is the lower heating value and ξ is the coefficient which is 1.06 for natural gas [34]. The composition of the natural gas used in the power plant is listed in Table 2.

3.2.3 Turbine [35]

$$\dot{E}_{\mathrm{D,Exp}} = \dot{E}_3 - \left(\dot{E}_4 + \dot{W}_{\mathrm{AC}}\right) \tag{24}$$

3.2.4 HRSG

$$\dot{E}_{\mathrm{D,HRSG}} = \dot{E}_5 + \dot{E}_9 + \dot{E}_{16} - \left(\dot{E}_6 + \dot{E}_{10} + \dot{E}_{12} + \dot{E}_{14}\right) \tag{25}$$

3.2.5 Steam turbine

$$\dot{E}_{\mathrm{D,GT}} = \dot{E}_{10} + \dot{E}_{13} - \left(\dot{E}_7 + \dot{E}_{11} + \dot{W}_{\mathrm{GT}}\right) \tag{26}$$

3.2.6 Condenser

$$\dot{E}_{\mathrm{D,Cond}} = \dot{E}_7 + \dot{E}_{17} - \left(\dot{E}_8 + \dot{E}_{18}\right) \tag{27}$$

3.2.7 A-W heat exchanger

$$\dot{E}_{\mathrm{D,A\text{-}W}} = \dot{E}_0 + \dot{E}_{15} - \left(\dot{E}_1 + \dot{E}_{16}\right) \tag{28}$$

3.3 Economic analysis

3.3.1 Daily fossil fuel saving

The IAH technology can significantly reduce the fossil fuel consumption, the fossil fuel saving (m_{saving}) can be calculated by the daily fuel consumption difference of conventional CCPP system (m_{con}) and the CCPP-IAH system (m_{IAH}):

$$m_{\mathrm{saving}} = m_{\mathrm{con}} - m_{\mathrm{IAH}} \tag{29}$$

3.3.2 Annual economic benefit

The annual economic benefit (P) can be calculated basing on the daily fossil fuel saving ($m_{\mathrm{saving}\text{-}i}$) and the fuel price ($p_i$) and it is assumed that there are 365 days through a year.

$$P = \sum_{i=1}^{i=365} p_i m_{\mathrm{saving}\text{-}i} \tag{30}$$

3.3.3 Payback period of project investment

The dynamic payback period of project investment (a) can be calculated by the division of total investment (I) and the annual economic benefit (P):

$$a = \mathrm{I}/P \tag{31}$$

Table 2.

The compositions of natural gas.

Ingredient	Value (%)
CH_4	94.2081
C_2H_6	2.9914
C_3H_8	0.4313
C_4H_{10}	0.1506
C_5H_{12}	0.0536
C_6H_{14}	0.0275
CO_2	1.8709
N_2	0.2639

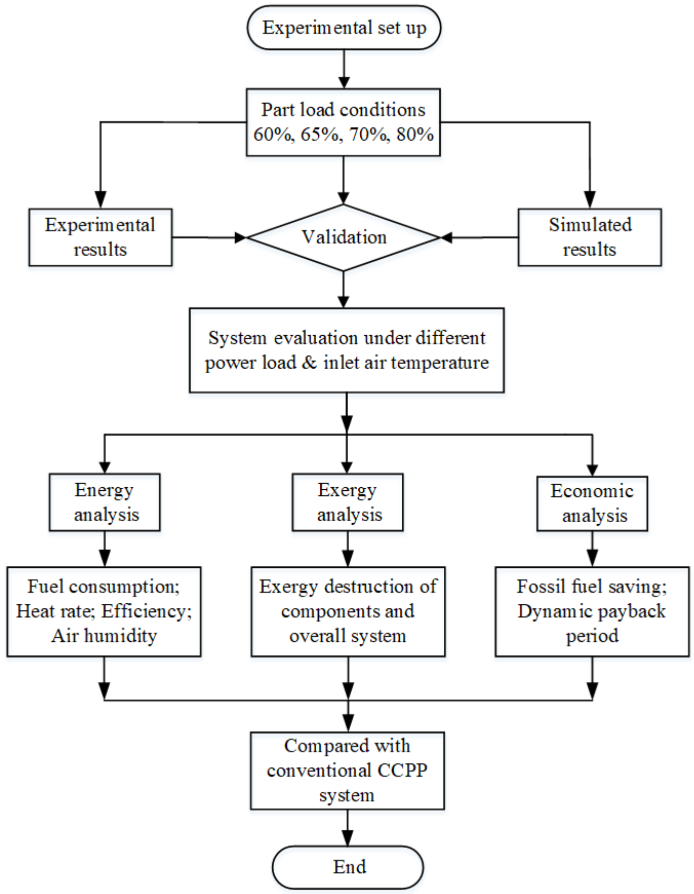

Figure 4. Methodology process of proposed CCPP-IAH system.

4. Experimental background and validation

4.1 The experimental background

The proposed CCPP-IAH system is located in Tianjin city, in the northern part of China, where the average temperature and the minimum temperature in winter is 277.8 K and 259.6 K, respectively. Tianjin is a coastal city, the average relative humidity is 56.4 %. Therefore, there may be freezing phenomenon occurring in the inlet air system (without an anti-freezing unit) which may result in increased pressure loss and lower power output in the winter. The annual temperature and air humidity of Tianjin city are from the meteorological database as shown in Figure 5.

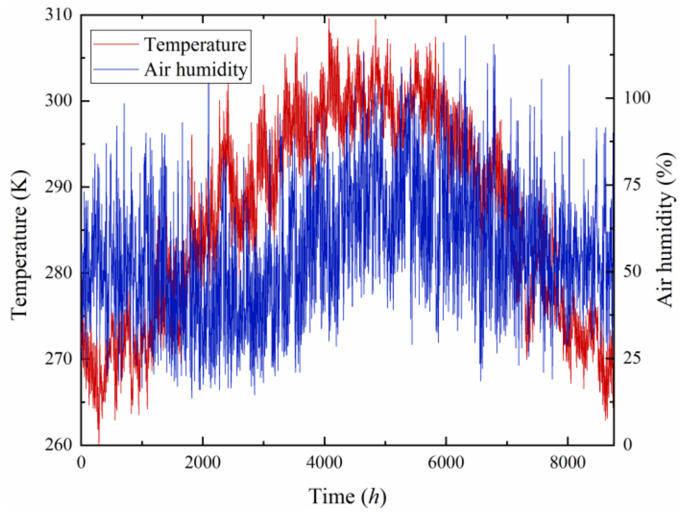

Figure 5. The annual temperature and relative air humidity of Tianjin city from the beginning January to end of December.

The purpose of this experimental test is to increase the *IAT* by 4 K in space heating season, and increase the *IAT* by 18 K during non-space heating season in part load conditions. The experimental test was carried out under part load conditions with ambient temperature of 289 K, air humidity of 61 % and the ambient pressure of 101.1kPa.

In addition, the thermal performance test of the facility followed the guidelines of ASME PTC 46-1996 [36]. The uncertainty of the measurement instruments based on the ASME PTC 19.1 [37]. The maximum allowable deviation of test parameters are shown in Table 3.

Table 3

The maximum allowable deviation of test parameters

Parameters	Allowable deviation
Ambient temperature	±2.0 K
Ambient pressure	±0.5 %
Natural gas pressure	±1.0 %
Power output	±2.0 %
Power factor	±2.0 %
Speed of revolution	±1.0 %
Exhaust gas pressure of GT	±1.0 %

4.2 Model validation

To better understand the performance of system components and the overall system under part load conditions, the proposed CCPP-IAH system is modeled by the Ebsilon Professional software. The software is developed by the German STEAG Electric Power Company (a sub-company of the Ruhr Group). The software is widely used in the area of design, simulation and optimization of power plants.

The experimental recorded and simulated values under part load conditions are listed in Table 4. It can be seen that the values show a good agreement. It is concluded that the models are validated and the performance of the main components as well as the overall CCPP-IAH plant can be deeper investigated. Also, the performance of inlet air humidity from experimental results is list in Table 5

Table 4

The comparison of experimental and simulated values.

Item	Unit	Load=65 %		Load=80 %	
		Exp.	Sim.	Exp.	Sim.
Inlet air temperature (T_1)	K	289.0	289.5	300.5	300.7
GT power output ($\dot{W}_{GT}$)	MW	77.7	77.4	101.4	100.5
ST power output ($\dot{W}_{ST}$)	MW	51.7	52.9	58.7	60.0
CCPP power output ($\dot{W}_{CCPP}$)	MW	129.4	130.0	160.0	160.1
Fuel consumption ($\dot{m}_f$)	kg/s	5.62	5.65	6.49	6.49
Heat rate ($\dot{H}_{CCPP}$)	kJ/kWh	7680.5	7642.2	7130.1	7128.0
GT efficiency (η_{GT})	%	28.14	28.05	31.98	31.70
CCPP efficiency (η_{CCPP})	%	46.87	47.11	50.49	50.51

Table 5

The performance of inlet air humidity from experimental results.

NO.	T_0 (K)	T_1 (K)	$T_1 - T_0$ (K)	φ_0 (%)	φ_1 (%)
1	285.3	293.3	8.0	87.4	62.3
2	286.0	295.0	9.0	85.9	54.4
3	287.0	297.3	10.3	80.3	50.2
4	287.2	297.5	10.3	79.2	48.6
5	289.9	302.7	12.8	60.6	42.7
6	289.5	308.3	18.8	62.1	30.7
7	288.9	308.3	19.4	64.7	31.3
8	288.5	310.5	22.0	64.8	30.3

5. Results and discussion

5.1 Part-load performance of the proposed CCPP-IAH system

Most gas-fired power plants are used for peak-shaving and are typically operating at part-load conditions. The purpose of the experimental test is to analysis the performance of the proposed CCPP-IAH system under part-load conditions and provide data for model validation. Based on the thermodynamic modeling and mathematical equations described above, the part-load performance of CCPP-IAH system is investigated in detail through simulation data.

In this section, the ambient temperature of 289 K, the air humidity of 90% were considered and the *IAT* was heated to about 303 K by the A-W exchanger using the recovered energy from HRSG. The part-load efficiencies of the proposed CCPP-IAH system and the conventional CCPP system (CS) are compared in Figure 6. It is noticed that the GT-efficiency and the overall system efficiency increase in line with the power for both system configurations. However, the GT efficiency is generally a little lower for the CCPP-IAH system while the HRSG efficiency is slightly increased due a higher *IAT*. More specifically, a higher *IAT* increases the power consumption of the compressor that is taken from the work produced by the expander. Nevertheless, for the whole system, the proposed CCPP-IAH system slightly increases the overall efficiency by 0.17 %, 0.16 %, 0.17 % and 0.23 % under the power loads of 60 %, 65 %, 70 % and 80 %, respectively.

The heat rate refers to the fuel heat input per kilowatt hour electricity produced. It is a fundamental index used to determine the thermal economy of power plants. A lower value is preferred. The heat rate of the GT as well as the proposed CCPP-IAH system at part load conditions are seen in Figure 7. It is found that the GT heat rate of the CCPP-IAH system is higher than that of the CS system, due to its lower thermal efficiency at the higher *IAT*. Yet, the overall heat rate shows slightly lowered values of 29.3 kJ/kWh, 27.1 kJ/kWh, 25.1 kJ/kWh and 43.9 kJ/kWh at the different system loads.

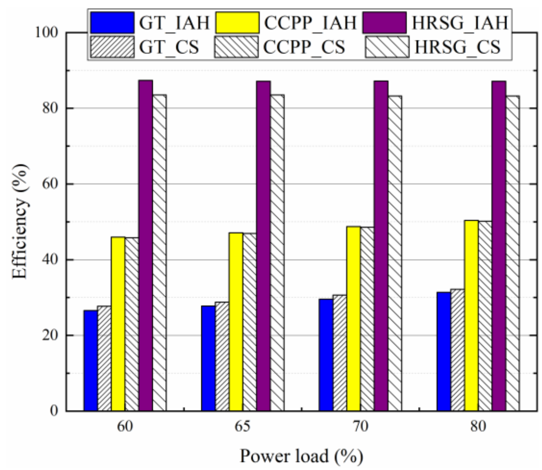

Figure 6. The efficiencies for proposed CCPP-IAH system under part load conditions.

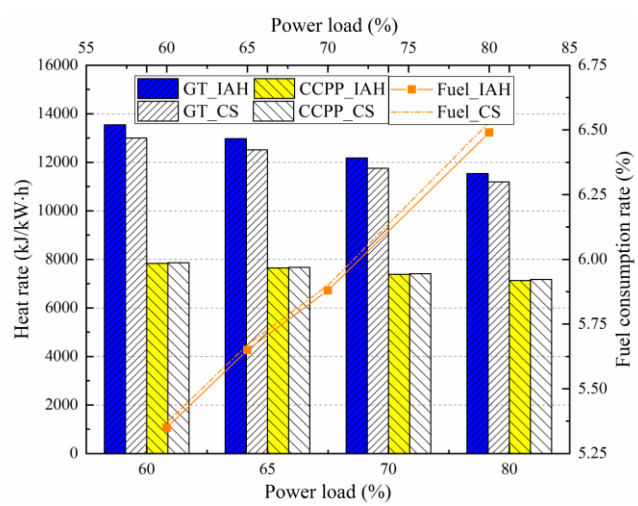

Figure 7. The heat rate for proposed CCPP-IAH system under part load conditions

Additionally, the exergy destruction of system components under part load conditions are presented in Figure 8. Among the individual components, the combustion chamber (CC) contributes the highest exergy destruction. However, at the power load of 60 %, the exergy destruction of the CC drops from 82.5 MW ($E_{\mathrm{D,CC}}^{\mathrm{CS}}$) to 80.0 MW ($E_{\mathrm{D,CC}}^{\mathrm{IAH}}$) since the IAH configuration supply more energy through the heated inlet air, that in turn reduces the fuel consumption. The air compressor (AC), expander (Exp), steam turbine (ST) and the condenser (Cond) of the CCPP-IAH system reveal a slightly higher exergy destruction than in the CS system. Nevertheless, the total exergy destruction (or irreversible energy loss) of the CCPP-IAH system is lower than the CS system under the part load conditions. This can be explained by the utilizing of low-grade energy at the end of the HRSG which is better recovered and utilized by the topping Brayton cycle and the bottoming Rankine cycle.

Additionally, the components of the proposed system are further divided into two parts: The Brayton cycle (AC, CC and Exp) and the Rankine cycle (ST, HRSG and Cond) to gain a better understanding of the performance of the applied components. Accordingly, it is clear that both Brayton cycle part and Rankine cycle part show improvement trends due to the IAH technology applied in the system.

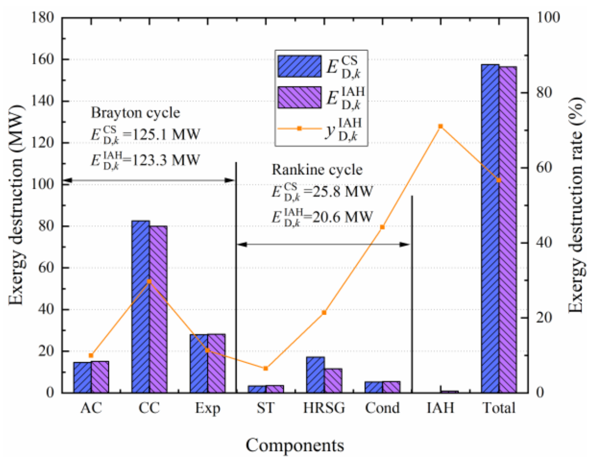

(a) Power load of 60%

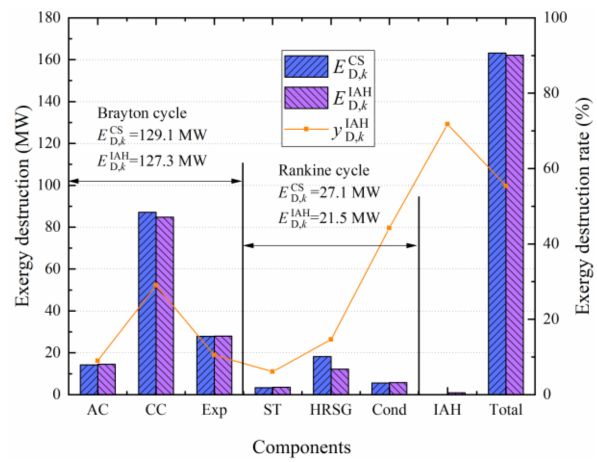

(b) Power load of 65%

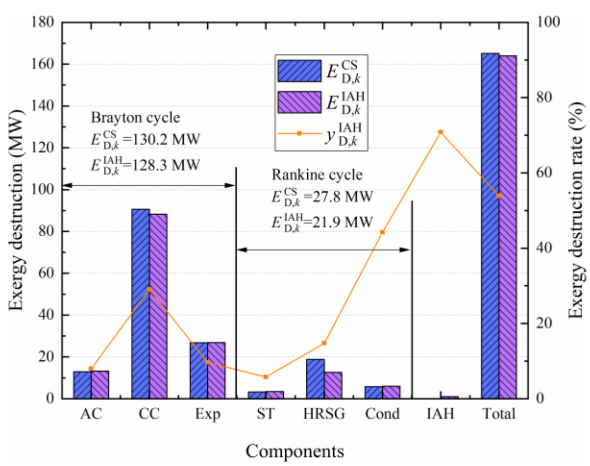

(c) Power load of 70%

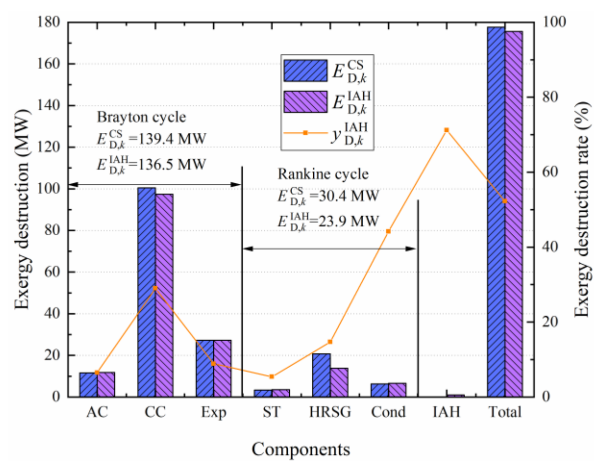

(d) Power load of 80%

Figure 8. Exergy destruction of components under part load conditions.

5.2 The effect of inlet air heating on the proposed CCPP-IAH system

The effect of inlet air heating on the proposed CCPP-IAH system is examined in this section. Figure 9 demonstrates the rate of fuel consumption of the CCPP-IAH system under the selected part load conditions. It is shown that while the *IAT* increases, the fuel consumption reduces slightly. The reason being, that low-grade waste energy at the end of the HRSG is further recovered and utilized by both the Brayton cycle and the Rankine cycle in the proposed IAH configuration.

The trends in Figure 9 are also obtained experimentally as the fuel consumption decreased from 5.67 kg/s (*IAT* of 286.7 K, ~129.4 MW) to 5.65 kg/s (*IAT* of 303.2 K, ~129.4 MW) at the power load of 65 %. In addition, the fuel consumption decreased from 6.52 kg/s (*IAT* of 291.4 K, 160.0 MW) to 6.49 kg/s (*IAT* of 302.3 K, 159.9 MW) at the power load of 80 %.

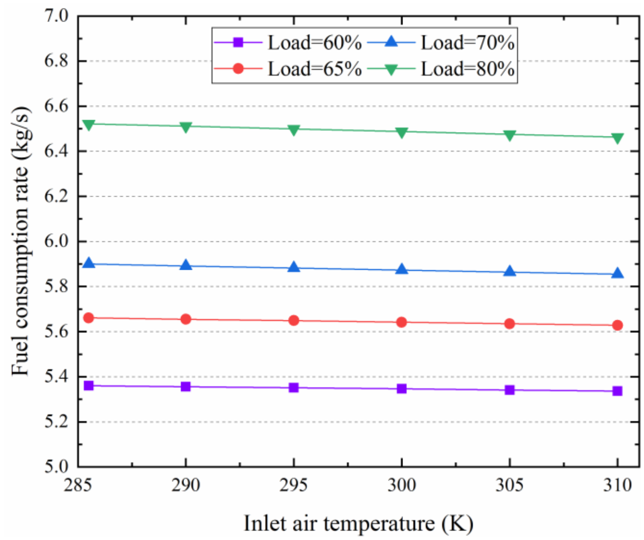

Figure 9. The fuel consumption rate of proposed CCPP-IAH system under part load conditions.

The change in inlet air humidity with respect to temperature of the proposed CCPP-IAH system under part load conditions is shown in Figure 10. In the simulations, the ambient air humidity is 90 %. When heated by the A-W, the humidity decreases to 30 % when the *IAT* is 303 K as seen in the figure. This has a huge benefit to the operation of GT-based power plants in wintertime. The issue of ice and humidity blockages in the inlet air system is suppressed which minimizes inlet pressure losses that in turn reduce the power output of the combined cycle.

Besides, from the experimental results (Table 5) and simulated results (Figure 10) we can obtain that the increased temperature of inlet air drops the air humidity and the IAH technology can significantly avoid the abovementioned issues.

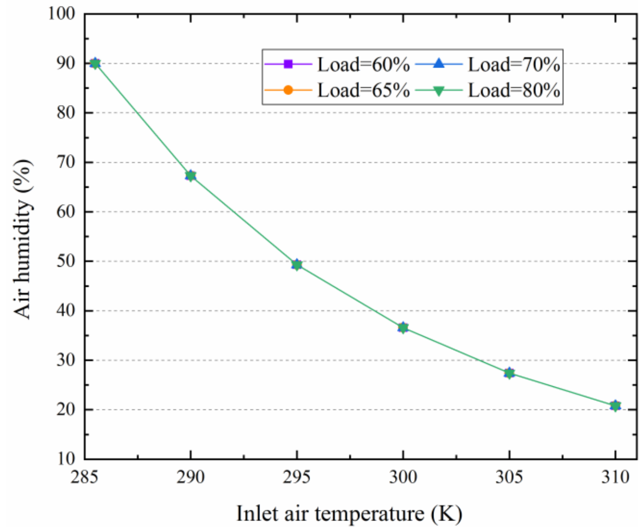

Figure 10. The air humidity of proposed CCPP-IAH system under part load conditions.

The effect of the heated inlet air on the GT-, HRSG- and overall CCPP system efficiencies are illustrated in Figure 11. A higher *IAT* provides a lower GT thermal efficiency. On the other hand, the heated inlet air (from the recovered energy in the HRSG) will act to improve the efficiencies for the HRSG itself as well as the overall system performance.

Herein, from the results of experimental test, the overall plant efficiency increased from 46.73 % (*IAT* of 286.7 K, ~129.4 MW) to 46.87 % (*IAT* of 303.2 K, ~129.4 MW) under the power load of 65 %. And it increased from 50.22 % (*IAT* of 291.4K, 160.0 MW) to 50.48 % (*IAT* of 302.4 K, 159.9 MW) under the power load of 80 %.

The heat rates of the GT and overall plant at different inlet air temperature are depicted in Figure 12. It is shown that the heat rate of the GT increases with the higher *IAT*, however , the overall heat rate of CCPP-IAH system reduces slightly. This matches the experimental results where the heat rate dropped from 7168.6 kJ/kWh (*IAT* of 291.4 K, 160.0 MW) to 7131 kJ/kWh (*IAT* of 302 K, 159.9 MW) under the power load of 80 %.

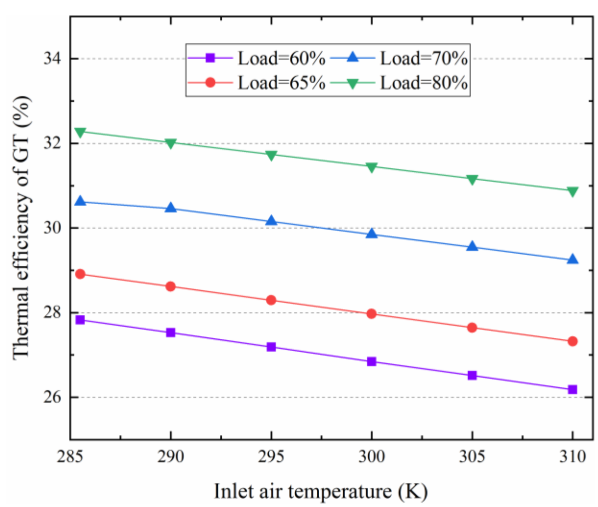

(a)

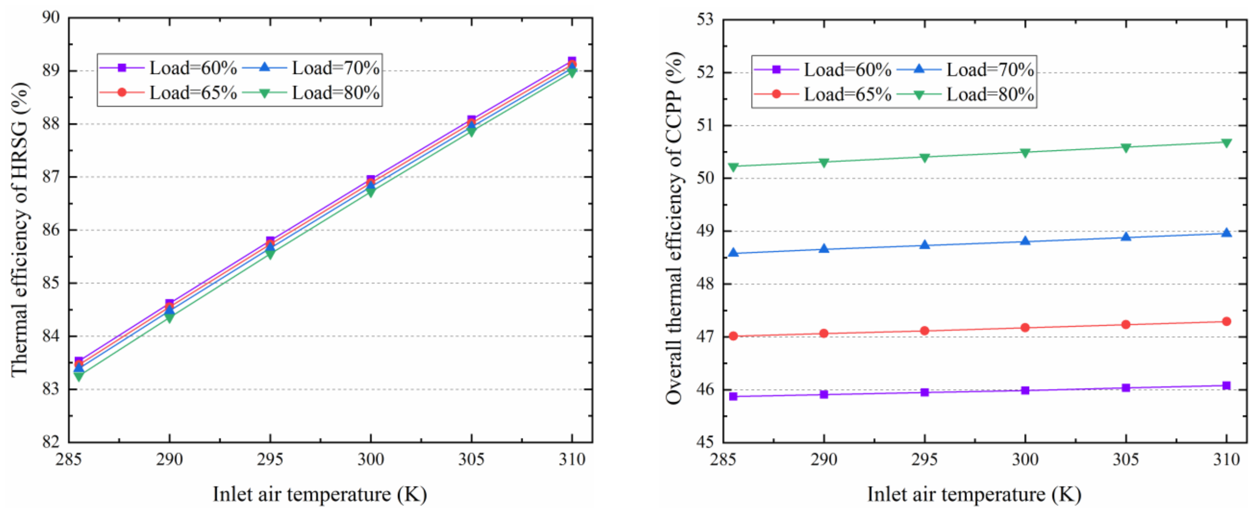

(b) (c)

Figure 11. Brayton cycle components performances under different *IAT*.

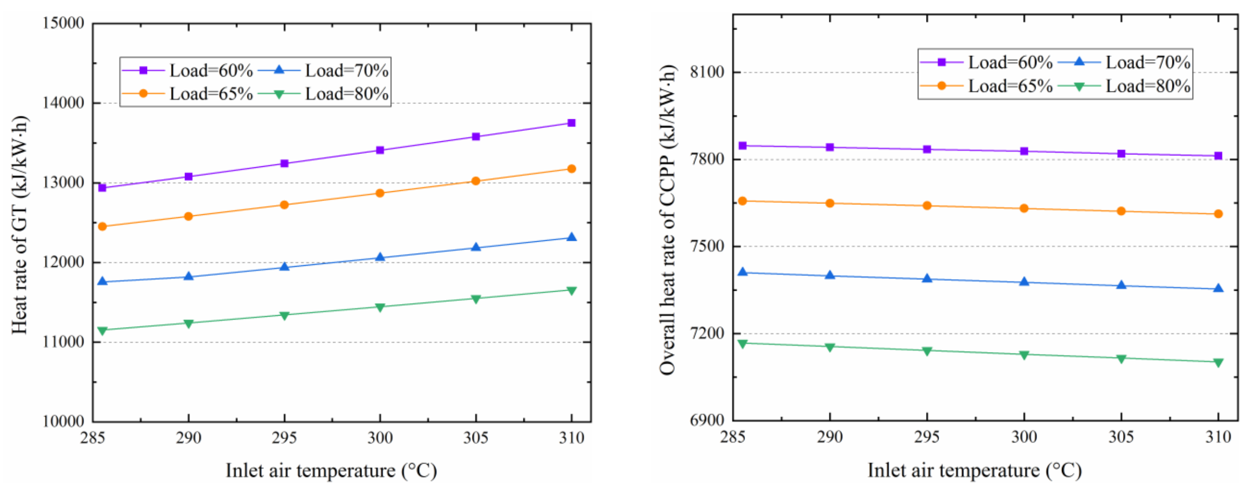

(a) (b)

Figure 12. The heat rates of GT and overall plant under different *IAT*.

The exergy destruction of main components (Brayton cycle and Rankine cycle) under different *IAT* conditions are shown in Figure 13. The components that are most affected the by the *IAT* are the AC, CC and HRSG. The exergy destruction of the AC increases in line with the *IAT*, as it will consume more useful work to compress the air. The exergy destruction of CC is the largest and it exhibits a downtrend with the *IAT* increasing, obviously. For the reason that a higher *IAT* will contribute higher inlet compressed air temperature, thus reduce part of fossil fuel consumption which is used to improve the flue gas temperature in CC. That is to say, a part of irreversible energy loss of CC is significantly avoided due to the higher inlet compressed air temperature. Moreover, the energy utilized to raise the *IAT* is collected by the W-G exchanger in HRSG, as shown in Figure 1, and a higher *IAT* will take more energy away from HRSG, therefore the “energy loss” for HRSG increases and leads a higher exergy destruction.

Additionally, it is clearly illustrated that a higher *IAT* will contribute lower exergy destruction for the Brayton cycle and cause larger exergy destruction for Rankine cycle. For instance, the exergy destruction drops from 124.6MW (290 K) to 122.5MW (310 K), while the exergy destruction increases from 18.9 MW (290 K) to 21.6 MW (310 K) respectively under the power load of 60 %. However, the overall plant exergy destruction will decrease with the *IAT* increasing. Thus, the IAH technology has a positive achievement in both improving the overall system thermal efficiency and reducing the exergy destruction.

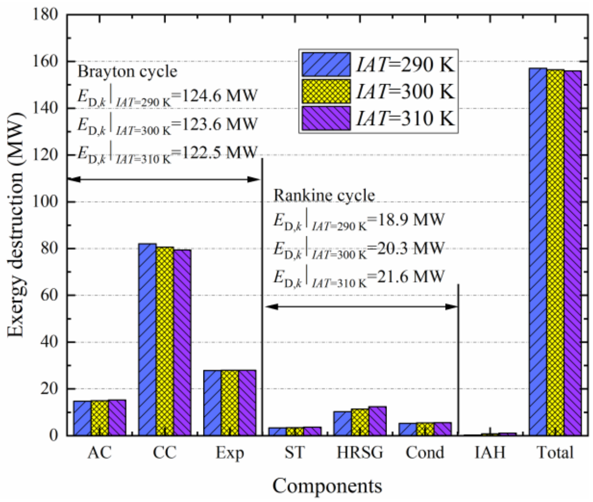

(a) Power load of 60%

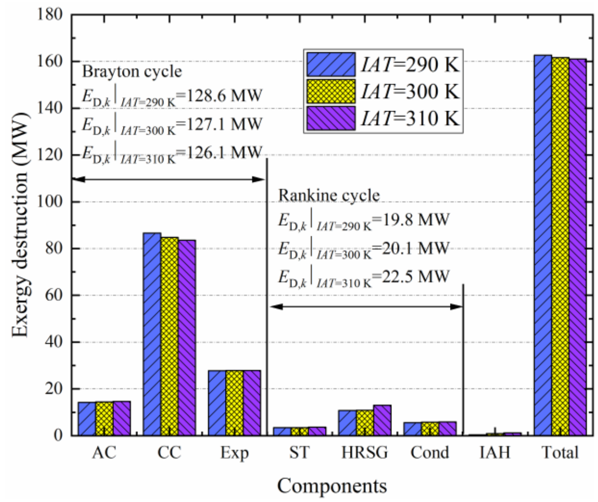

(b) Power load of 65%

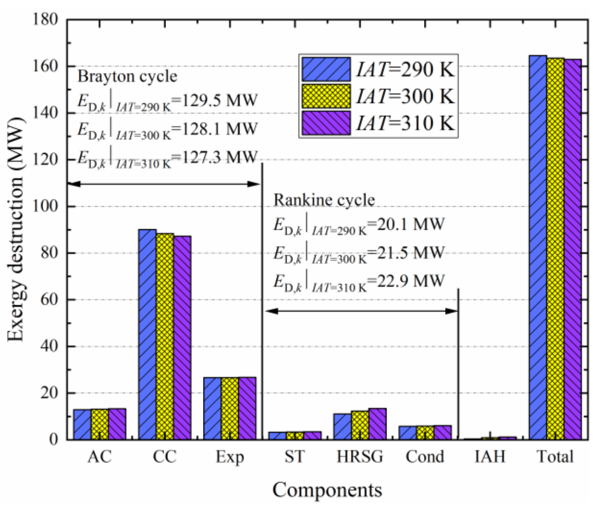

(c) Power load of 70%

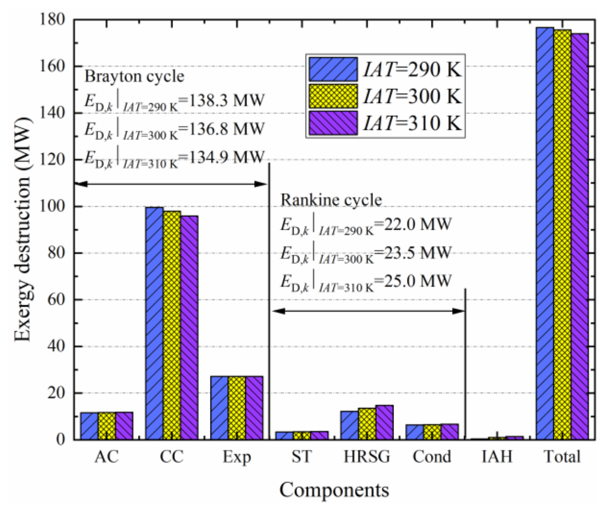

(d) Power load of 80%

Figure 13. Exergy destruction of components under different *IAT*.

The daily fossil fuel saving under different power load and different *IAT* conditions is presented in Figure 14. It can been seen that the daily fossil fuel saving (natural gas) raises from 0 ton/day (*IAT* of 285 K) to 2.7 ton/day (*IAT* of 310 K) under the power load of 65 % and it raises from 0 ton/day (*IAT* of 285 K) to 5.1 ton/day (*IAT* of 310 K) under the power load of 80 %. Besides, it is reported by the Guodian Science and Technology Research Institute , China Energy Investment Corporation [38] that the proposed CCPP-IAH system can significantly improve the efficiency of CCPP by more than 0.89 % under the part-load conditions [39]. Additionally, the annual economic benefit from energy saving is more than \$ 5.88×10^{5} and the payback period of project investment is less than 3 years [39].

Furthermore, the application of this IAH technology not only improves the part-load efficiency of the CCPP, but also effectively solves the problems of ice and humidity blockages in the inlet air system and significantly enhances the operation safety of the CCPP under complex meteorological conditions [39].

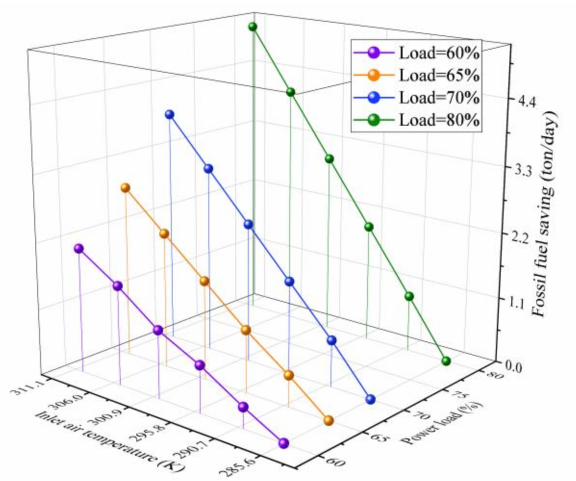

Figure 14. The fossil fuel saving under different power load and *IAT* conditions.

6. Conclusion

In this paper, a CCPP with inlet air heating (CCPP-IAH) system is proposed to solve the issues of ice and humidity blockages of inlet air system in winter climate. The model is established in the software of Ebsilon and is validated by experimental results. The performance of the CCPP-IAH system under part load conditions is analyzed experimentally and by simulation methods. Important conclusions are summarized:

- With heated inlet air the GT efficiency is lower than conventionally (without heated inlet air), Nevertheless the overall plant efficiency of the proposed CCPP-IAH system achieves a higher efficiency besides a lower heat rate compared to the conventional system. In addition, the heated inlet air by the recovered energy in the HRSG raises the HRSG efficiency.

- The proposed system reduces the fuel consumption slightly from 5.67 kg/s to 5.65 kg/s and from 6.52 kg/s to 6.49 kg/s at 65 % and 80 % power load respectively. Moreover, the inlet air humidity will decrease from 90 % to 30 % under the heated *IAT* of 303 K, which is of great significance to the operation of gas-fired power plants in wintertime.

- From the exergy analysis, the CC produces most of the exergy destruction in the system that, however, reduces with the *IAT* in contrast to the AC and HRSG components. Moreover, for both the Brayton cycle part and the Rankine cycle part, the exergy destruction will decrease with the IAH application.

- The daily fossil fuel will raise up to 2.9 ton/day (*IAT* of 310 K) and to 5.1 ton/day (*IAT* of 310 K) under the power load of 65 % and 80 %, respectively. In addition, from the reported economic analysis, the proposed CCPP-IAH system can significantly improve the efficiency of CCPP by more than 0.89 % under the part load conditions. The annual economic benefit from energy saving is more than \$ 5.88×10^5 and the payback period of project investment is less than 3 years.

Acknowledgement

This study was financially supported by the Natural Science Foundation of Beijing (3162030) and the Fundamental Research Funds for the Central Universities (2018QN035). The technical support was provided by the Guodian Science and Technology Research Institute, China Energy Investment Corporation. The authors are grateful for the contributions of Anders Ivarsson**,** reviewers and editors for giving valuable comments.

Nomenclature and Abbreviations

Abbreviations

AC	Air compressor
A-W	Air-Water heat exchanger
CC	Combustion chamber
CCPP	Combined cycle power plant
GT	Gas turbine
HRSG	Heat recovery steam generator
IAH	Inlet air heating
IAT	Inlet air temperature
ST	Steam turbine
W-G	Water-Gas heat exchanger

Roman symbols

c_{pa}	Specific heat of air, J/(kg·K)
c_{pg}	Specific heat of turbine exhaust gas, J/(kg·K)
$\dot{E}_{\mathrm{D},k}$	Exergy destruction of *k*th component, kJ/kg
$\dot{E}_{\mathrm{F},k}$	Fuel exergy of *k*th component, kJ/kg
$\dot{E}_{\mathrm{P},k}$	Product exergy of *k*th component, kJ/kg
$\dot{E}_{\mathrm{D,AC}}$	Exergy destruction rate of air compressor, kJ/kg
$\dot{E}_{\mathrm{D,CC}}$	Exergy destruction rate of combustion chamber, kJ/kg
$\dot{E}_{\mathrm{fuel}}$	Exergy destruction rate of fossil fuel, kJ/kg
$\dot{E}_{\mathrm{D,Exp}}$	Exergy destruction rate of expander, kJ/kg
$\dot{E}_{\mathrm{D,HRSG}}$	Exergy destruction rate of HRSG, kJ/kg
$\dot{E}_{\mathrm{D,GT}}$	Exergy destruction rate of gas turbine, kJ/kg
$\dot{E}_{\mathrm{D,Cond}}$	Exergy destruction rate of condenser, kJ/kg
$\dot{E}_{\mathrm{D,A\text{-}W}}$	Exergy destruction rate of air-water heat exchanger, kJ/kg
$\dot{E}_0$	Exergy destruction rate of ambient temperature, kJ/kg
$\dot{E}_1$	Exergy destruction rate of inlet air of air compressor, kJ/kg
$\dot{E}_2$	Exergy destruction rate of outlet compressed air, kJ/kg

$\dot{E}_3$ Exergy destruction rate of fossil fuel, kJ/kg

$\dot{E}_4$ Exergy destruction rate of outlet exhaust gas of CC, kJ/kg

$\dot{E}_5$ Exergy destruction rate of exhaust gas of gas turbine, kJ/kg

$\dot{E}_6$ Exergy destruction rate of exhaust gas of HRSG, kJ/kg

$\dot{E}_7$ Exergy destruction rate of the outlet steam of low-pressure steam, kJ/kg

$\dot{E}_8$ Exergy destruction rate of outlet water of condenser, kJ/kg

$\dot{E}_9$ Exergy destruction rate of feed water, kJ/kg

$\dot{E}_{10}$ Exergy destruction rate of high-pressure steam, kJ/kg

$\dot{E}_{11}$ Exergy destruction rate of the outlet steam of high-pressure steam, kJ/kg

$\dot{E}_{12}$ Exergy destruction rate of superheated low-pressure steam, kJ/kg

$\dot{E}_{13}$ Exergy destruction rate of low-pressure steam, kJ/kg

$\dot{E}_{14}$ Exergy destruction rate of heated water from water-gas heat exchanger, kJ/kg

$\dot{E}_{15}$ Exergy destruction rate of inlet water of air-water heat exchanger, kJ/kg

$\dot{E}_{16}$ Exergy destruction rate of outlet water of air-water heat exchanger, kJ/kg

$\dot{E}_{17}$ Exergy destruction rate of inlet water of condenser, kJ/kg

$\dot{E}_{18}$ Exergy destruction rate of outlet water of condenser, kJ/kg

h_2 The entropy of outlet compressed air, kJ/kg

h_4 The entropy of outlet gas of the CC, kJ/kg

h_5 The entropy of the flue gas from gas turbine, kJ/kg

h_6 The entropy of the exhaust gas of HRSG, kJ/kg

h_7 The entropy of the outlet steam of low-pressure steam, kJ/kg

h_8 The entropy of outlet water of condenser, kJ/kg

h_{10} The entropy of high-pressure steam, kJ/kg

h_{11} The entropy of the outlet steam of high-pressure steam, kJ/kg

h_{13} The entropy of low-pressure steam, kJ/kg

h_{15} The entropy of inlet water of air-water heat exchanger, kJ/kg

h_{16} The entropy of outlet water of air-water heat exchanger, kJ/kg

h_{17} The entropy of inlet water of condenser, kJ/kg

h_{18} The entropy of outlet water of condenser, kJ/kg

$\dot{H}_{GT}$ Heat rate of gas turbine, kJ/kWh

$\dot{H}_{CCPP}$ Heat rate of combined cycle power plant, kJ/kWh

LHV_f Lower heating value of fossil fuel, kJ/kg

$\dot{m}_a$ Mass flow rate of inlet air, kg/s

$\dot{m}_f$ Mass flow rate of fossil fuel, kg/s

$\dot{m}_g$ Mass flow rate of exhaust gas, kg/s

$\dot{m}_5$ Mass flow rate of the flue gas from gas turbine, kg/s

$\dot{m}_6$ Mass flow rate of the exhaust gas of HRSG, kg/s

$\dot{m}_7$ Mass flow rate of the outlet steam of low-pressure steam, kg/s

$\dot{m}_8$ Mass flow rate of outlet water of condenser, kg/s

$\dot{m}_{10}$ Mass flow rate of high-pressure steam, kg/s

$\dot{m}_{11}$ Mass flow rate of the outlet steam of high-pressure steam, kg/s

$\dot{m}_{13}$ Mass flow rate of low-pressure steam, kg/s

$\dot{m}_{15}$ Mass flow rate of inlet water of air-water heat exchanger, kg/s

$\dot{m}_{16}$ Mass flow rate of outlet water of air-water heat exchanger, kg/s

$\dot{m}_{17}$ Mass flow rate of inlet water of condenser, kg/s

$\dot{m}_{18}$ Mass flow rate of outlet water of condenser, kg/s

P_1 Inlet air pressure of the air compressor, MPa

P_2 Out air pressure of the air compressor, MPa

T_0 Ambient temperature, K

T_1 Inlet air temperate of the air compressor, K

T_2 Outlet air temperature of the air compressor, K

T_4 The exhaust gas of combustion chamber, K

T_5 The outlet temperature of the turbine, K

$\dot{W}_{AC}$ Power consumed by air compressor, MW

$\dot{W}_{GT}$ Produced work by expander, MW

$\dot{W}_{ST}$ Power output of the steam turbine, MW

Greek symbols

η_{AC} Air compressor efficiency, %

η_{CC} Combustion chamber efficiency, %

η_{CCPP} Combined cycle power plant efficiency, %

η_{Exp} Expander efficiency, %

η_{GT} Gas turbine efficiency, %

η_{HRSG} Heat recovery steam generator efficiency, %

r_{AC} Pressure ratio, %

$y_{D,k}$ Exergy destruction rate of *k*th component, %

ξ The coefficient of fuel exergy

References

[1] IEA. World energy outlook 2017. Organization for Economic Co-operation and Development; 2017.

[2] Iglesias Garcia S, Ferreiro Garcia R, Carbia Carril J, Iglesias Garcia D. Critical review of the first-law efficiency in different power combined cycle architectures. Energy Conversion and Management. 2017;148:844-59.

[3] Kalina J. Analysis of alternative configurations of heat recovery process in small and medium scale combined cycle power plants. Energy Conversion and Management. 2017;152:13-21.

[4] Yingjian L, Abakr YA, Qi Q, Xinkui Y, Jiping Z. Energy efficiency assessment of fixed asset investment projects – A case study of a Shenzhen combined-cycle power plant. Renewable and Sustainable Energy Reviews. 2016;59:1195-208.

[5] Ibrahim Tk, Mohammed MK, Awad OI, Rahman MM, Najafi G, Basrawi F, et al. The optimum performance of the combined cycle power plant: A comprehensive review. Renewable and Sustainable Energy Reviews. 2017;79:459-74.

[6] Blumberg T, Assar M, Morosuk T, Tsatsaronis G. Comparative exergoeconomic evaluation of the latest generation of combined-cycle power plants. Energy Conversion and Management. 2017;153:616-26.

[7] Ibrahim TK, Basrawi F, Awad OI, Abdullah AN, Najafi G, Mamat R, et al. Thermal performance of gas turbine power plant based on exergy analysis. Applied Thermal Engineering. 2017;115:977-85.

[8] Maheshwari M, Singh O. Comparative evaluation of different combined cycle configurations having simple gas turbine, steam turbine and ammonia water turbine. Energy. 2019;168:1217-36.

[9] Sanaye S, Amani M, Amani P. 4E modeling and multi-criteria optimization of CCHPW gas turbine plant with inlet air cooling and steam injection. Sustainable Energy Technologies and Assessments. 2018;29:70-81.

[10] Mohapatra AK, Sanjay. Exergetic evaluation of gas-turbine based combined cycle system with vapor absorption inlet cooling. Applied Thermal Engineering. 2018;136:431-43.

[11] Haglind F. Variable geometry gas turbines for improving the part-load performance of marine combined cycles – Gas turbine performance. Energy. 2010;35:562-70.

[12] Li Y, Zhang G, Bai Z, Song X, Wang L, Yang Y. Backpressure adjustable gas turbine combined cycle: A method to improve part-load efficiency. Energy Conversion and Management. 2018;174:739-54.

[13] El-Shazly AA, Elhelw M, Sorour MM, El-Maghlany WM. Gas turbine performance enhancement via utilizing different integrated turbine inlet cooling techniques. Alexandria Engineering Journal. 2016;55:1903-14.

[14] Huang Z, Yang C, Yang H, Ma X. Off-design heating/power flexibility for steam injected gas turbine based CCHP considering variable geometry operation. Energy. 2018;165:1048-60.

[15] Moon SW, Kwon HM, Kim TS, Kang DW, Sohn JL. A novel coolant cooling method for enhancing the performance of the gas turbine combined cycle. Energy. 2018;160:625-34.

[16] Shukla AK, Singh O. Thermodynamic investigation of parameters affecting the execution of steam injected cooled gas turbine based combined cycle power plant with vapor absorption inlet air cooling. Applied Thermal Engineering. 2017;122:380-8.

[17] Rahman AAA, Mokheimer EMA. Boosting gas turbine combined cycles in hot regions Using inlet air cooling including solar energy. Energy Procedia. 2017;142:1509-15.

[18] Baakeem SS, Orfi J, Al-Ansary H. Performance improvement of gas turbine power plants by utilizing turbine inlet air-cooling (TIAC) technologies in Riyadh, Saudi Arabia. Applied Thermal Engineering. 2018;138:417-32.

[19] Kotowicz J, Brzęczek M, Job M. The thermodynamic and economic characteristics of the modern combined cycle power plant with gas turbine steam cooling. Energy. 2018;164:359-76.

[20] Kwon HM, Kim TS, Sohn JL, Kang DW. Performance improvement of gas turbine combined cycle power plant by dual cooling of the inlet air and turbine coolant using an absorption chiller. Energy. 2018;163:1050-61.

[21] Liu Z, Karimi IA, He T. A novel inlet air cooling system based on liquefied natural gas cold energy utilization for improving power plant performance. Energy Conversion and Management. 2019;187:41-52.
[22] https://www.steag-systemtechnologies.com/en/products/ebsilon-professional/.
[23] Ersayin E, Ozgener L. Performance analysis of combined cycle power plants: A case study. Renewable and Sustainable Energy Reviews. 2015;43:832-42.
[24] Şen G, Nil M, Mamur H, Doğan H, Karamolla M, Karaçor M, et al. The effect of ambient temperature on electric power generation in natural gas combined cycle power plant—A case study. Energy Reports. 2018;4:682-90.
[25] Saghafifar M, Gadalla M. Innovative inlet air cooling technology for gas turbine power plants using integrated solid desiccant and Maisotsenko cooler. Energy. 2015;87:663-77.
[26] Memon AG, Memon RA. Thermodynamic analysis of a trigeneration system proposed for residential application. Energy Conversion and Management. 2017;145:182-203.
[27] Król J, Ocłoń P. Economic analysis of heat and electricity production in combined heat and power plant equipped with steam and water boilers and natural gas engines. Energy Conversion and Management. 2018;176:11-29.
[28] Liao G, Liu L, Zhang F, Jiaqiang E, Chen J. A novel combined cooling-heating and power (CCHP) system integrated organic Rankine cycle for waste heat recovery of bottom slag in coal-fired plants. Energy Conversion and Management. 2019;186:380-92.
[29] Pattanayak L, Padhi BN. Thermodynamic analysis of combined cycle power plant using regasification cold energy from LNG terminal. Energy. 2018;164:1-9.
[30] Katulić S, Čehil M, Schneider DR. Exergoeconomic optimization of a combined cycle power plant's bottoming cycle using organic working fluids. Energy Conversion and Management. 2018;171:1721-36.
[31] Singh OK. Performance enhancement of combined cycle power plant using inlet air cooling by exhaust heat operated ammonia-water absorption refrigeration system. Applied Energy. 2016;180:867-79.
[32] Udeh GT, Udeh PO. Comparative thermo-economic analysis of multi-fuel fired gas turbine power plant. Renewable Energy. 2019;133:295-306.
[33] Hosseini SE, Barzegaravval H, Ganjehkaviri A, Wahid MA, Mohd Jaafar MN. Modelling and exergoeconomic-environmental analysis of combined cycle power generation system using flameless burner for steam generation. Energy Conversion and Management. 2017;135:362-72.
[34] Ameri M, Mokhtari H, Mostafavi Sani M. 4E analyses and multi-objective optimization of different fuels application for a large combined cycle power plant. Energy. 2018;156:371-86.
[35] Anvari S, Taghavifar H, Parvishi A. Thermo- economical consideration of Regenerative organic Rankine cycle coupling with the absorption chiller systems incorporated in the trigeneration system. Energy Conversion and Management. 2017;148:317-29.
[36] https://www.asme.org/products/codes-standards/ptc-46-1996-overall-plant-performance.
[37] https://www.asme.org/products/codes-standards/ptc-191-2013-test-uncertainty.
[38] http://www.ceic.com/.
[39] https://mp.weixin.qq.com/s/xxjnnipTjILSQSMq9wyGTA.